Modeling of the Formation of Under-Riser Macrosegregation during Solidification of Binary Alloys

Q.Z. DIAO and H.L. TSAI

The formation of macrosegregation in a rectangular ingot with reduced cross section from the riser to the casting, chilled from the bottom, has been studied numerically. In addition to positive inverse segregation occurring near the chilled surface, very severe negative segregation around the under-riser region and moderate positive segregation near the top corners of the casting were found. Although large circulating vortexes are created by natural convection in the under-riser region during the early stage of solidification, the fluid flow in the mushy zone is dominated by solidification shrinkage. As a result, the final solute distribution in the casting is determined by the flow of solute-rich liquid in the mushy zone owing to the combined effects of solidification shrinkage and change of cross section from casting to riser. Detailed explanations regarding the effect of different flow phenomena on the formation of the segregations are provided. The effects of riser size and cooling condition at the bottom of the ingot on the formation of macrosegregation also were studied. The predicted negative and positive macrosegregations in the casting compared very well with the available experimental data.

I. INTRODUCTION

IN a solidified ingot, the existence of a large-scale nonuniformity in composition (*i.e.*, macrosegregation) can significantly change its mechanical and chemical properties. Once this casting defect is formed, it is nearly impossible to eliminate, leading to a costly remelt and recast process. In the past, many experimental studies[1,2] employing various metals or simulated metals (*e.g.*, NH_4Cl-H_2O) have been conducted to investigate how macrosegregation is formed. Today, it can be said that the mechanisms leading to the formation of macrosegregation have been well understood.[3] These include the floating or settling of equiaxed grains and/or detached dendrites in the mushy zone and the flow of solute-rich or solute-poor liquid in the mushy zone. Complex fluid-flow phenomena in a solidifying casting can have many causes, including solidification contraction, forced convection due to external forces (*e.g.*, magnetic force), natural convection due to thermal gradients, natural convection due to solutal gradients, and surface tension force (*i.e.*, Marangoni effect). Depending upon casting conditions, one or a combination of several of these factors could result in the formation of many kinds of macrosegregation, including inverse segregation, banding segregation, ghost bands, under-riser segregation, freckles, channel segregation, A- or V-segregation, and centerline segregation.[3]

As the simplest fluid-flow phenomena that can be obtained in a solidifying casting are under the condition of unidirectional solidification (UDS) cooled from the bottom, many early experimental and theoretical investigations[4,5] on the formation of macrosegregation in castings have concentrated on UDS. Perhaps one of the most important contributions in the early stages of macrosegregation study was made by Flemings and coworkers.[6,7,8] Flemings and Nereo[6] developed the well-known "local solute redistribution equation" and considered explicitly the effect of shrinkage-induced flow on the formation of macrosegregation. However, they did not consider solute diffusion in their equation, and the fluid-flow velocity and the movement of liquidus and solidus isotherms were either assumed or measured. In spite of these limitations, they used the equation to successfully predict the formation of inverse segregation, segregation resulting from cross-section change, under-riser positive segregation, and centerline segregation.[7,8] Mehrabian *et al.*[9] extended the Flemings' model to include the effects of gravity acting on a fluid of variable density. Darcy's law was used to describe two-dimensional (2-D) velocity and pressure field; however, the temperature gradients and solidification rate were prescribed without solving the energy equation. Fujii *et al.*[10] made an attempt to improve the model to solve the mass, momentum, and energy equations in the mushy zone, but in their model, the mushy zone was uncoupled from the solid and liquid regions, and the calculation was confined to the case with planar liquid and solid fronts. In fact, it can be said that before approximately 1987, the theoretical modeling of macrosegregation was limited by the lack of availability of a mathematical model and associated numerical technique to handle coupled multidimensional heat transfer, fluid flow, and mass transfer in a solidifying casting.

One important step in the modeling of solidification processes was made when the "continuum formulation" was introduced in about 1987. Beckermann and Viskanta[11] and Bennon and Incropera[12] employed the volumetric averaging technique or classical mixture theory to derive the continuum formulation, in which the mushy zone was treated as a porous medium, and the

Q.Z. DIAO, Graduate Student, and H.L. TSAI, Associate Professor of Mechanical Engineering, are with the Department of Mechanical and Aerospace Engineering and Engineering Mechanics, University of Missouri-Rolla, Rolla, MO 65401.

Manuscript submitted June 21, 1993.

solid and liquid phases were the special states of mushy zone, having zero and infinite permeability, respectively. Hence, only a set of governing differential equations was required for the entire domain, including the liquid phase, mushy zone, and solid phase. With the continuum model, the formation of V-segregation and freckles during multidimensional solidification of aqueous NH_4Cl system have been successfully predicted.[13] However, in the continuum formulation, with the exception of the buoyancy terms, a constant density was assumed for the solid and liquid phases, and as a result, the solidification shrinkage was neglected. Chiang and Tsai[14,15] improved the model by including the shrinkage effect in the momentum equations and studied the shrinkage-induced flow and its interaction with natural convection during solidification of Fe-Cr alloys. The model later was extended by Diao and Tsai[16,17] to include the species equation, and it successfully predicted the formation of inverse segregation for UDS of an aluminum-copper alloy cooled from the bottom.

The aim of the present work is to extend the model[16,17] to the effect of casting geometry with a reduced cross section from the riser to the casting on the formation of macrosegregation. Under this condition, more complex flow phenomena, including both shrinkage-induced fluid flow and natural convection, are present. The effects of fluid flow due to natural convection and solidification shrinkage, which is further complicated by the change of cross section, on the formation of macrosegregation are of particular interest.

II. ANALYSES

The continuum formulation, including the shrinkage effect previously developed by Diao and Tsai,[16,17] will be employed in the present study. The assumptions used to derive the equations and the meanings of each term in the equation have been discussed previously;[16] hence, they will not be repeated here. For solidification of a 2-D casting, the continuity, momentum, energy, and species equations may be expressed as

Continuity

$$\frac{\partial}{\partial t}(\rho) + \nabla \cdot (\rho \mathbf{V}) = 0 \qquad [1]$$

Momentum

$$\frac{\partial}{\partial t}(\rho u) + \nabla \cdot (\rho \mathbf{V} u) = \nabla \cdot \left(\mu_l \frac{\rho}{\rho_l} \nabla u\right) - \frac{\partial p}{\partial x} - \frac{\mu_l}{K} \frac{\rho}{\rho_l} (u - u_s) - \frac{C\rho^2}{K^{1/2}\rho_l} |u - u_s| (u - u_s) - \nabla \cdot (\rho f_s f_l \mathbf{V}_r u_r) + \nabla \cdot \left(\mu_l u \nabla\left(\frac{\rho}{\rho_l}\right)\right) \qquad [2]$$

$$\frac{\partial}{\partial t}(\rho v) + \nabla \cdot (\rho \mathbf{V} v) = \nabla \cdot \left(\mu_l \frac{\rho}{\rho_l} \nabla v\right) - \frac{\partial p}{\partial y} - \frac{\mu_l}{K} \frac{\rho}{\rho_l} (v - v_s) - \frac{C\rho^2}{K^{1/2}\rho_l} |v - v_s| (v - v_s) - \nabla \cdot (\rho f_s f_l \mathbf{V}_r v_r) + \nabla \cdot \left(\mu_l v \nabla\left(\frac{\rho}{\rho_l}\right)\right) + \rho g(\beta_T (T - T_0) + \beta_s (f_l^\alpha - f_{l,0}^\alpha)) \qquad [3]$$

Energy

$$\frac{\partial}{\partial t}(\rho h) + \nabla \cdot (\rho \mathbf{V} h) = \nabla \cdot \left(\frac{k}{c_s} \nabla h\right) + \nabla \cdot \left(\frac{k}{c_s} \nabla (h_s - h)\right) - \nabla \cdot (\rho(\mathbf{V} - \mathbf{V}_s)(h_l - h)) \qquad [4]$$

Species

$$\frac{\partial}{\partial t}(\rho f^\alpha) + \nabla \cdot (\rho \mathbf{V} f^\alpha) = \nabla \cdot (\rho D \nabla f^\alpha) + \nabla \cdot (\rho D \nabla (f_l^\alpha - f^\alpha)) - \nabla \cdot (\rho(\mathbf{V} - \mathbf{V}_s)(f_l^\alpha - f^\alpha)) \qquad [5]$$

In Eqs. [1] through [5], the continuum density, specific heat, thermal conductivity, mass diffusivity, solid mass fraction, liquid mass fraction, velocity, enthalpy, and mass fraction of constituent α are defined as follows:

$$\rho = g_s\rho_s + g_l\rho_l; \qquad c = f_s c_s + f_l c_l; \qquad k = g_s k_s + g_l k_l$$

$$D = f_s D_s + f_l D_l; \qquad f_s = \frac{g_s\rho_s}{\rho}; \qquad f_l = \frac{g_l\rho_l}{\rho}$$

$$\mathbf{V} = f_s \mathbf{V}_s + f_l \mathbf{V}_l; \qquad h = f_s h_s + f_l h_l; \qquad f^\alpha = f_s f_s^\alpha + f_l f_l^\alpha \qquad [6]$$

If the phase-specific heats are assumed constant, the phase enthalpy for the solid and liquid can be expressed as

$$h_s = c_s T; \qquad h_l = c_l T + (c_s - c_l) T_e + H \qquad [7]$$

where H is the latent heat of the alloy.

The assumption of permeability function in the mushy zone requires consideration of the growth morphology specific to the alloy under study. In the present study, the permeability function analogous to fluid flow in the porous media is assumed, employing the Carman-Kozeny equation[18,19]

$$K = \frac{g_l^3}{c_1(1 - g_l)^2}; \qquad c_1 = \frac{180}{d^2} \qquad [8]$$

where d is proportional to the dendrite dimension, which is assumed to be a constant and is on the order of 10^{-2} cm. The inertial coefficient, C, can be calculated from[20]

$$C = 0.13 g_l^{-3/2} \qquad [9]$$

Closure of the system of conservation equations requires supplementary relations. With the assumption of local thermodynamic equilibrium, the required relations may be obtained from the equilibrium phase diagram. Neglecting curvature of the solidus and liquidus lines in the phase diagram, the solid mass fraction, as well as solid and liquid phase compositions, can be expressed as

$$f_s = \frac{1}{1 - k_p}\left[\frac{T - T_l}{T - T_m}\right];$$

$$f_s^\alpha = \left[\frac{k_p}{1 + f_s(k_p - 1)}\right] f^\alpha;$$

$$f_l^\alpha = \left[\frac{1}{1 + f_s(k_p - 1)}\right] f^\alpha \qquad [10]$$

where T_l is the liquidus temperature corresponding to f^α, T_m is the fusion temperature when $f^\alpha = 0$, and the equilibrium partition ratio, k_p, is the ratio of the slopes for the liquidus and solidus lines.

In the governing differential equations (Eqs. [1] through [5]), there is a solid-phase velocity. The solid-phase velocity is associated with the movement of precipitated, solid, equiaxed grains and/or broken dendrites in the mushy zone. Generally speaking, there are certain relations between the solid-phase and liquid-phase velocities;[21] however, the exact formulas are not known at this time. Also, for UDS cooled from the bottom, employed in the present study, the solid phase is likely to be stationary. Hence, the solid-phase velocity is assumed to be zero in the present study, and the equations are simplified accordingly.

Figure 1 shows the geometry of the casting, including the riser used in the present study. An aluminum-copper alloy with constant initial copper concentration and temperature is solidified by extracting heat from the bottom of the casting through a chill, while the other boundaries are kept adiabatic. In the mathematical modeling, an effective convective heat-transfer coefficient, h_c, is used between the casting and the chill. Due to symmetry of the domain, only the right half of the casting is used in the calculation.

The coupled continuity, momentum, energy, and species equations, subject to the required boundary conditions, were solved by an implicit, control volume-based, finite difference procedure using the SIMPLEC algorithm. The domain change due to solidification shrinkage was handled by the front tracking method. Detailed discussion about the numerical method and the check of numerical accuracy were given in the previous article.[16]

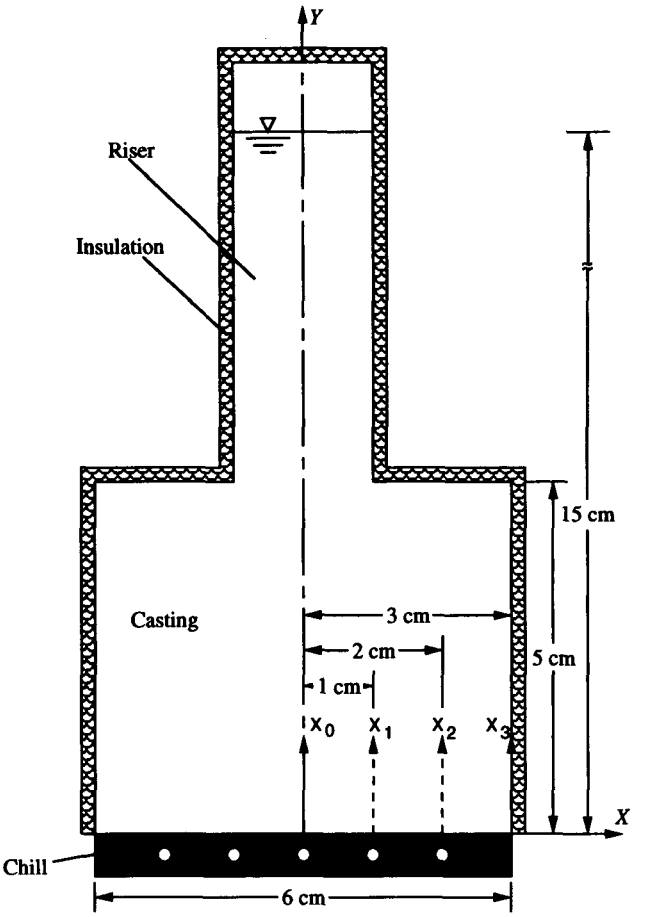

Fig. 1—Schematic representation of the physical domain and the dimensions.

III. RESULTS AND DISCUSSION

A. *Temperature, Velocity, and Solute Distributions*

Numerical calculations were performed for the solidification of Al-4.68 wt pct Cu alloys with the geometry and its dimensions as sketched in Figure 1. The thermophysical properties of aluminum-copper alloys[16] and casting conditions used in the present study are summarized in Table I. During solidification, the height of the riser decreases;[14,15] however, as we are interested in the phenomena occurring in the casting, only part of the riser (5-cm height) will be shown in the Figures.

Figures 2, 3, and 4 show the temperature, velocity, and solute distributions in the casting at times of 25, 55, and 75 seconds, respectively. The solidus and liquidus fronts also are shown in the velocity figures, indicating the interfaces between the solid phase and the mushy zone and between the mushy zone and the liquid phase. In the early stage of solidification, as shown in Figure 2(a), the region below the riser is still in liquid phase, and the isotherms are horizontal except near the riser, at which they are distorted due to the feeding of hotter metal from the riser. For the same horizontal positions from the chilled surface, the higher temperature below the riser creates temperature gradients leading to the formation of a clockwise vortex (as viewed on the right half of the symmetry plane). It is noted that the natural convection at the bottom of the riser is upward and that this flow is strong enough to overcome the downward fluid flow caused by the shrinkage effect. Figure 2(b) shows the solute distribution in the casting at a time of 25 seconds, and more detailed, time-dependent solute distribution along different axes (X_0, X_1, X_2, and X_3 in Figure 1) will be discussed next. It is

Table I. Thermophysical Properties of Al-4.68 Wt Pct Cu and Casting Conditions

c_s	solid specific heat (J g^{-1} K^{-1})	1.0928
c_l	liquid specific heat (J g^{-1} K^{-1})	1.0588
D_s	solid solute diffusion coefficient (cm^2 s^{-1})	≈0
D_l	liquid solute diffusion coefficient (cm^2 s^{-1})	3×10^{-5}
k_s	solid thermal conductivity (W cm^{-1} K)	1.9249
k_l	liquid thermal conductivity (W cm^{-1} K)	0.8261
k_p	equilibrium partition ratio	0.170
ρ_s	solid density (g cm^{-3})	2.65
ρ_l	liquid density (g cm^{-3})	2.40
β_T	thermal expansion coefficient (K^{-1})	4.95×10^{-5}
β_s	solutal expansion coefficient	−2.0
μ	dynamic viscosity (g cm^{-1} s^{-1})	0.03
H	latent heat (J g^{-1})	397.5
T_e	eutectic temperature (K)	821.2
T_m	fusion temperature (K)	933.2
$f_{l,0}^{w}$	initial copper concentration (pct)	4.68
T_0	initial alloy temperature (K)	970.0
T_c	chill temperature (K)	293.0
h_c	convective heat transfer coefficient (W cm^{-2} K^{-1})	0.08

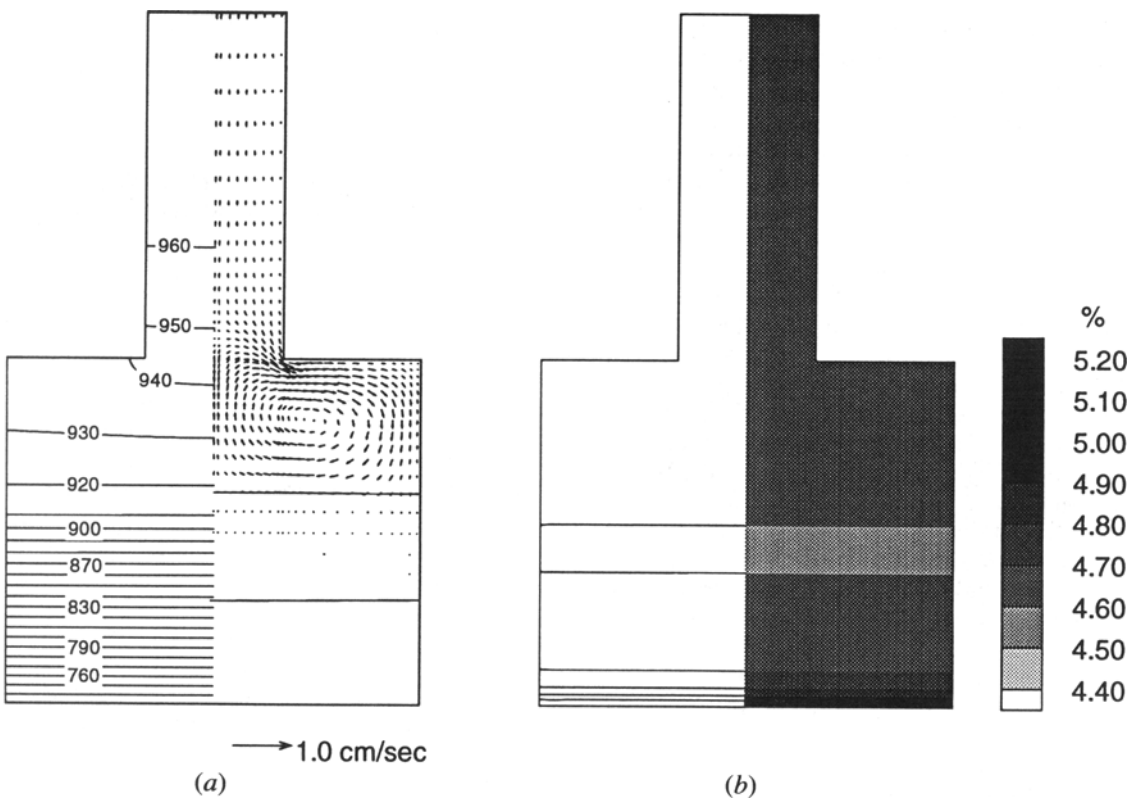

Fig. 2—(*a*) Isotherms (°K) and velocity vectors; and (*b*) isoconcentrations (pct Cu). t = 25 s.

seen that there is a higher solute concentration in the solidified casting near the chilled surface (which is commonly called inverse segregation), and the isoconcentrations are horizontal everywhere. As the heavier copper solute is rejected during solidification, and the vortex is not strong enough to entrain the rejected solute upward from the mushy zone, the solute concentration in the liquid phase below the riser remains uniform and the same as the initial value, as shown in Figure 2(b). Hence, in the lower portion of the casting both the temperature and solute concentration distributions can be considered one-dimensional. In other words, in the early stage of solidification, although there exists a vortex in the liquid phase due to temperature gradients as a result of the presence of the riser, the characteristics of temperature and solute distributions in the casting are similar to UDS without cross-sectional change, as discussed previously by Diao and Tsai.[16]

Figure 3(a) shows that at a time of 55 seconds, the entire under-riser region is in the mushy state, and the

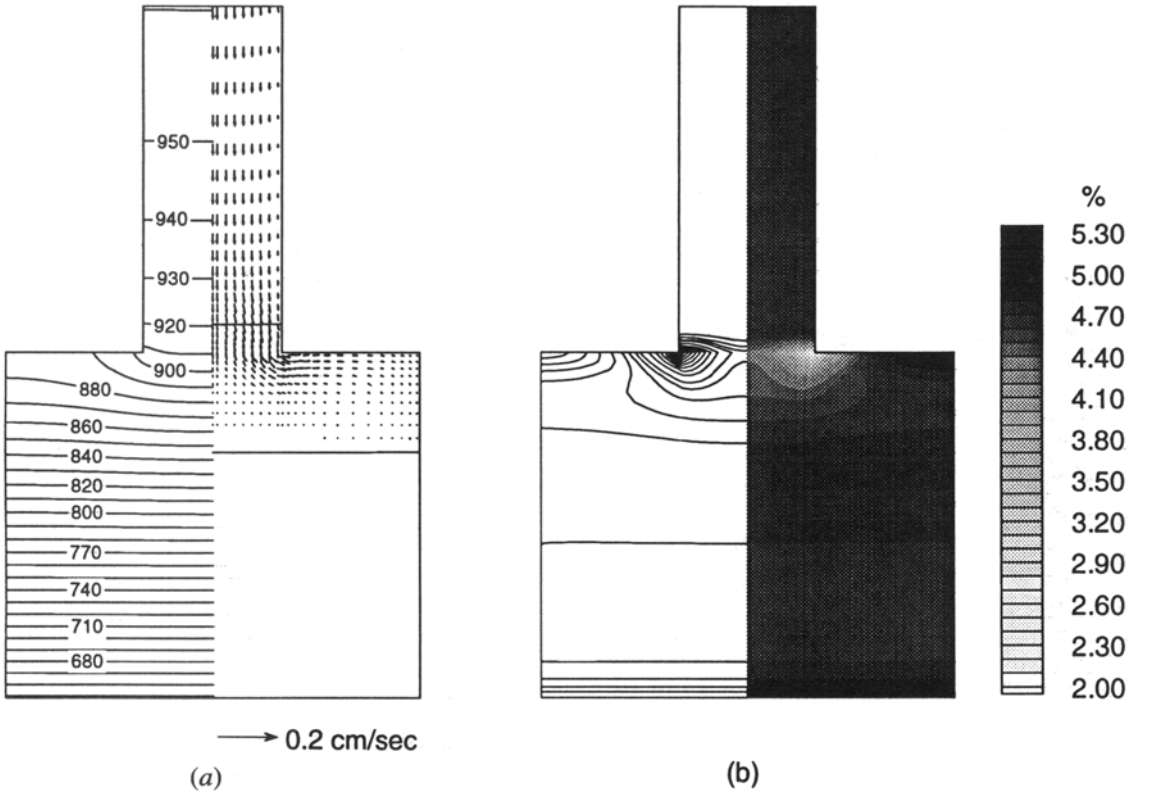

Fig. 3—(*a*) Isotherms (°K) and velocity vectors; and (*b*) isoconcentrations (pct Cu). t = 55 s.

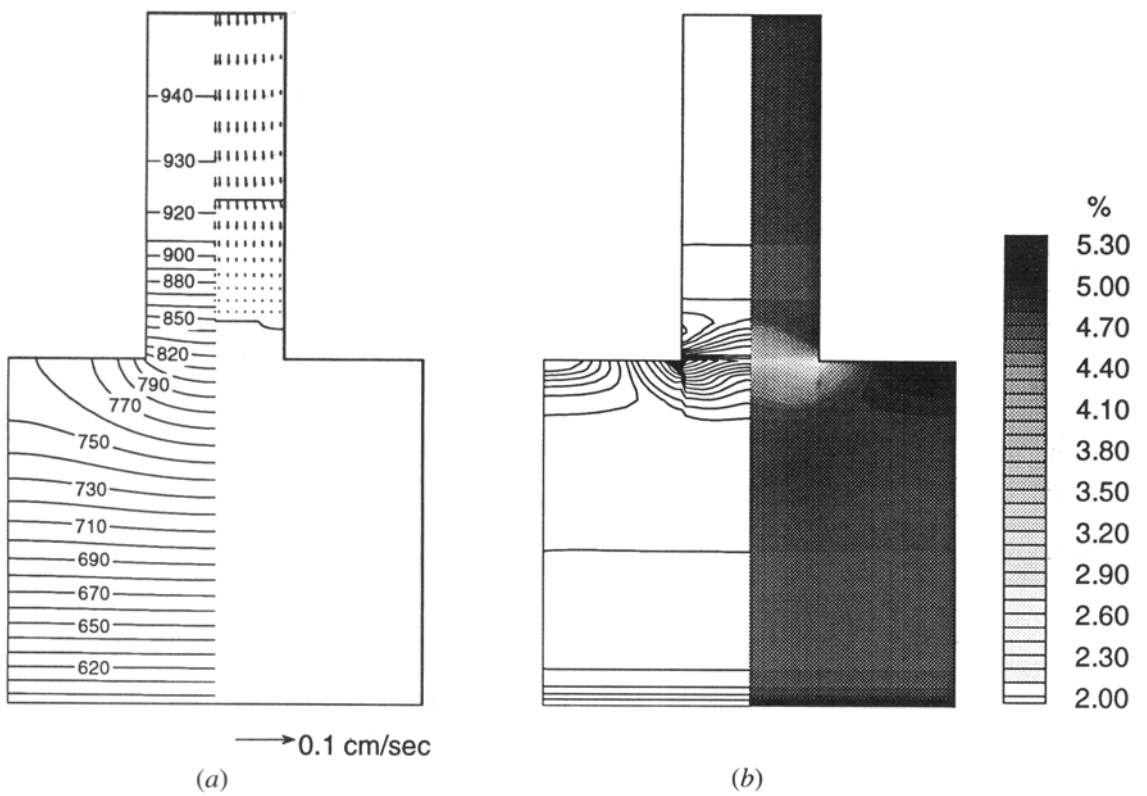

Fig. 4—(*a*) Isotherms (°K) and velocity vectors; and (*b*) isoconcentrations (pct Cu). t = 75 s.

vortex has disappeared. Because of the presence of the solid phase, fluid flow in the mushy zone near the casting-riser intersection is in the horizontal direction and toward the top corner of the casting. The rejected solute near the riser-casting region is "swept" by the interdendritic fluid and then discarded near the top corner of the casting, as the flow ceases near the "wall." Hence, negative segregation (*i.e.*, copper concentration is below the initial value) is formed around the under-riser region, while positive segregation (*i.e.*, copper concentration is above the initial value) is created near the top corner of the casting, as shown in Figure 3(b). Figure 4 shows the temperature, velocity, and solute concentration distributions when the casting is completely solidified. The inverse segregation near the chilled surface, the negative segregation around the under-riser region, and the positive segregation near the top corner of the casting can be clearly seen in the figure. Inverse segregation is a kind of positive segregation which occurs specifically near a chilled surface caused by solidification contraction.[6] It is interesting to see that the isotherms and isoconcentrations in the riser after the casting is completely solidified are uniform in the horizontal direction, which is similar to the results obtained when there is no cross-sectional change.[16]

In order to study in detail the process by which the macrosegregation is formed, time-dependent solute distributions along several vertical axes in the casting are given in Figure 5. For each curve in the figure, starting from the chill, there are three segments, corresponding to the solid phase, mushy zone, and liquid phase. It is seen that in addition to the inverse segregation adjacent to the chilled surface, there is a moving negative-segregated mushy zone, which has been previously discussed for UDS.[16] Next to the inverse segregation, the final solute distribution appears horizontal until about 2 cm from the chill, and thereafter it starts to be influenced by the presence of the riser. A profound negative segregation approximately centering the riser along either the X_0 or the X_1 axis is found, which apparently is caused by the change of the cross section. The severity of negative segregation along X_1 appears greater than along X_0, but the "band" is smaller. It is noted that the scale of the negative segregation is much greater than the inverse segregation and the positive- and negative-segregated bands discussed by Diao and Tsai.[17] After the casting is completely solidified, the solute distribution in the riser appears similar to UDS without cross-sectional change; *i.e.*, there is a moving negative-segregated mushy zone. The time-dependent solute distributions along X_2 and X_3 are similar to those along X_0 and X_1, with the exception that positive segregation is formed at the top shoulder of the casting near the corner (Figure 1).

The final solute distribution along the top surface of the casting (y = 5 cm) is shown in Figure 6. The solute decreases from the relative maximum at the center, point a, to the minimum at the intersection between the casting and the riser, point b, and then increases continuously along the shoulder of the casting to the maximum

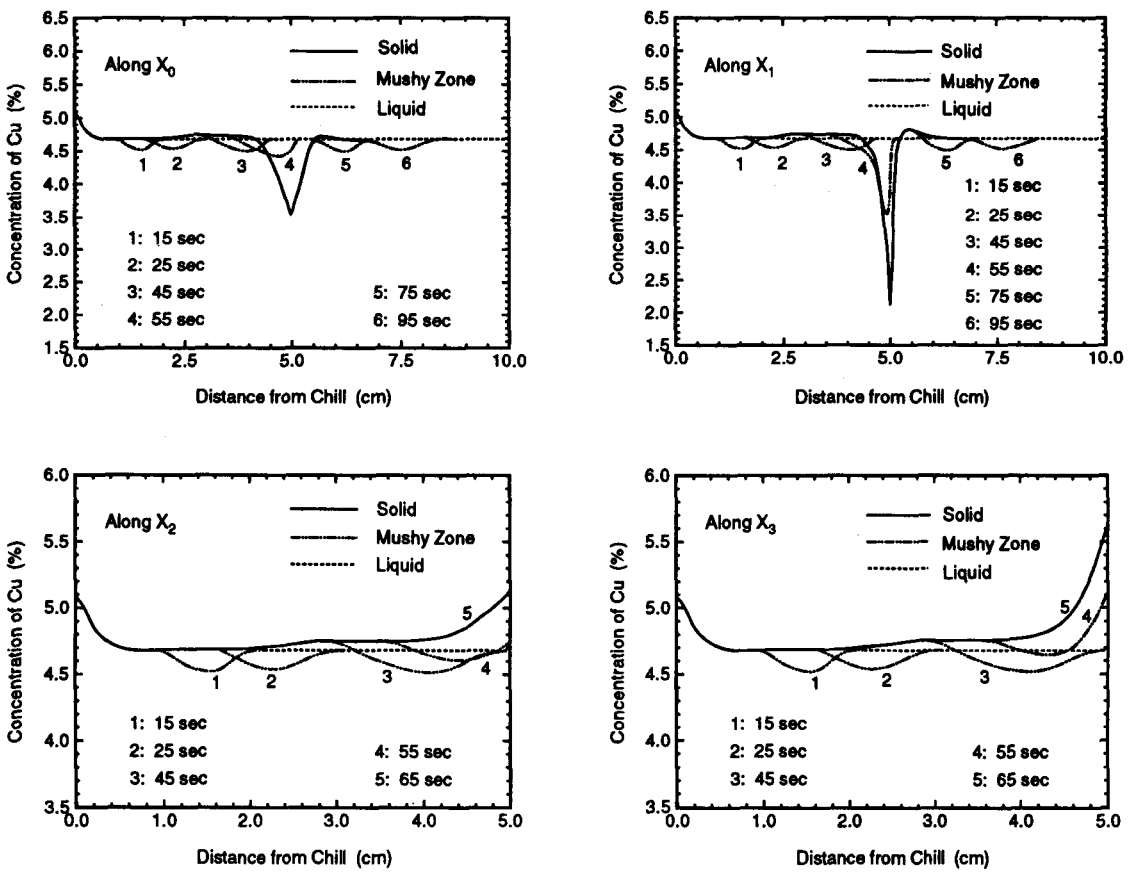

Fig. 5—Solute concentration distributions along axes X_0, X_1, X_2, and X_3 at different times.

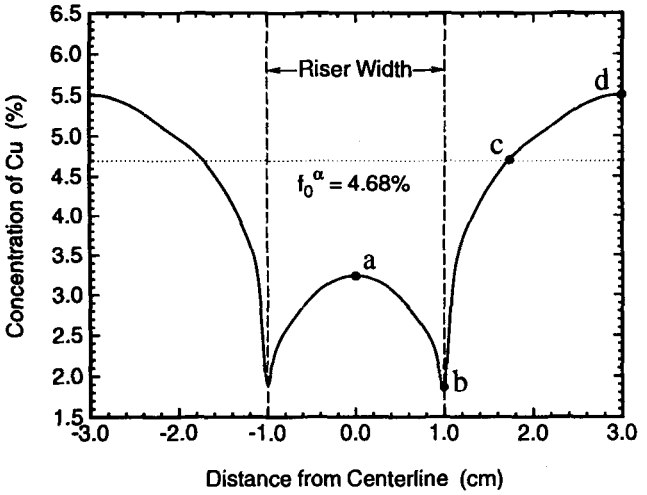

Fig. 6—Final solute concentration distribution along the top surface of the casting (y = 5 cm).

segregation at the corner, point d. Between points b and c, which is about one-third of the distance along the shoulder of the casting, the solute concentration is below the initial value; *i.e.*, negative segregation. It is seen that for an initial 4.6 pct Cu aluminum alloy, the minimum negative segregation is about 2.0 pct Cu, while the maximum positive segregation is about 5.6 pct Cu. Their difference is 3.6 pct, which is significant. In contrast, the inverse segregation is about 5.08 pct Cu, which is relatively less severe.

B. *Comparison with Previous Studies*

Figure 7 gives the comparison of the present predictions with the experimental results of Flemings and Nereo.[8] It is seen that the predicted positive inverse segregation, negative under-riser segregation, and positive top-corner segregation agree well with experimental data. The slight differences in the severity of the under-riser segregation between the predicted and experimental results could be due to the differences in alloy properties

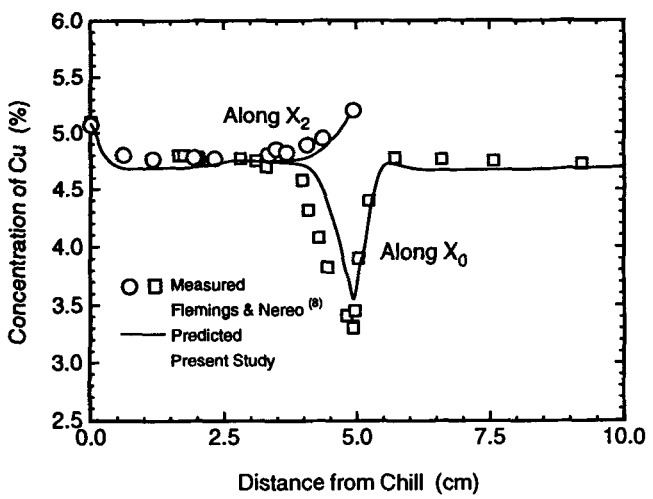

Fig. 7—Comparison between the predicted results and the data measured by Flemings and Nereo.[8]

and the cooling and casting conditions used, which were not given in the experimental work. Also, by reading Figures 5 and 6, we can see that along any axis between X_0 and X_1, the predicted results could be closer to the experimental data. In addition, the experimental data were obtained for a three-dimensional casting geometry, while the numerical simulation in the present study is performed for its 2-D projection. Nonetheless, the main features of the experimental results have been successfully predicted. Very similar solute distributions along the X_0 axis (Figure 5(a)) and along the top casting surface (Figure 6) are also predicted by Ohnaka and Matsumoto,[23] using a Fe-0.25 pct C alloy.

C. *Fluid Flow Affecting the Formation of Macrosegregation*

Under the conditions employed in the present study (cooled from the bottom with a heavier copper species rejected during solidification), the fluid flow occurring in the casting includes the natural convection due to temperature and concentration gradients and also includes shrinkage-induced flow. The flow phenomena are further complicated by the cross-sectional change from the riser to the casting. It is noted that the temperature gradients in the casting are induced by the externally imposed chill at the bottom of the casting, while the shrinkage-induced fluid flow is caused by the density (or specific volume) difference between the solid and liquid phases, which is naturally present in a solidifying system. In contrast, as the heavier copper species is rejected in the mushy zone during solidification starting from the bottom, stable solutal gradients will be created. Hence, the solutal gradients cannot themselves induce fluid flow, although they can "weaken" or "strengthen" the fluid flow caused by solidification shrinkage and/or temperature gradients, as discussed by Chen and Tsai.[22] Accordingly, in the following we will investigate the effects of shrinkage-induced flow and the natural convection induced by temperature gradients on the formation of macrosegregation.

1. *If the natural convection due to temperature gradients is neglected*

This corresponds to nullifying the thermal expansion coefficient, β_T, in Eq. [3] so that the possible natural convection due to temperature gradients is neglected in the mathematical modeling. Under this condition, the calculated fluid-flow patterns and solute distributions in the castings are shown in Figure 8. It is seen in Figure 8(a) that there is no vortex near the bottom of the riser, and the flow patterns are significantly different from those in Figure 2(a). However, comparing Figures 8(b) and 3(a), it is interesting to see that the flow patterns are nearly identical when the region between the casting and the riser is in the mushy state. The final solute distributions shown in Figures 8(c) and (d) indicating the macrosegregation in the casting are nearly the same as those given, respectively, in Figures 5 and 6.

2. *If the shrinkage-induced flow is neglected*

The shrinkage effect can be neglected if the last term and the second-to-last term on the right-hand side of Eqs. [2] and [3], respectively, are assumed to be zero.

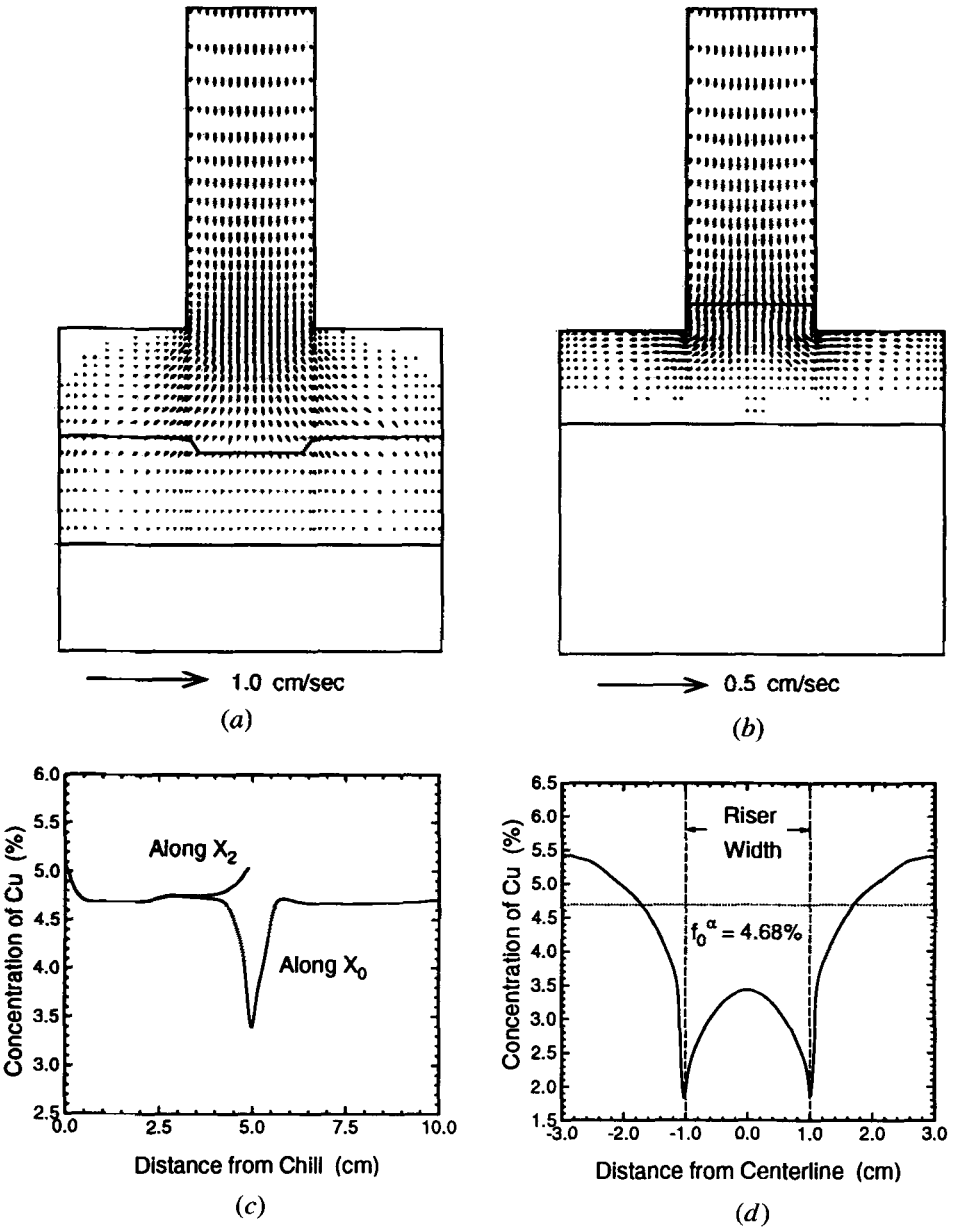

Fig. 8—Velocity vectors: (*a*) at t = 25 s and (*b*) at t = 55 s; and final solute concentration distributions: (*c*) along X_0 and X_2 axes and (*d*) along the top surface of the casting; if natural convection due to temperature gradients is neglected.

The average of the solid and liquid densities in Table I is used throughout the casting in the modeling. Figure 9 shows the flow patterns and solute distributions in the casting when the shrinkage effect is neglected. The flow patterns at a time of 25 seconds around the under-riser region (Figure 9(a)) are very similar to those shown in Figure 2(a); however, there is no fluid flow in the top portion of the riser. By comparing Figure 9(b) with Figures 3(a) and 8(b), we can conclude that the flow in the riser is mainly caused by the shrinkage effect, which can be understood easily, as possible natural convection is damped out by the smaller size of the riser. From Figure 9(b), at a time of 55 seconds, we can see that the solidification is faster when the shrinkage effect is neglected, compared with the corresponding Figures 3(a) and 8(b), because there is no hotter metal withdrawn downward from the riser due to solidification shrinkage. Figures 9(c) and (d) show that the solute distribution in the casting is nearly uniform and is the same as the initial solute concentration. This is because the natural convection in the liquid phase is not strong enough to entrain the rejected heavier copper species in the mushy zone located below. Hence, the natural convection due to temperature gradients under the conditions employed in the present study does not change the solute distribution in the casting.

From this discussion, we have the following conclusions: (1) the fluid flow in the mushy zone is dominated by shrinkage-induced flow, while in the liquid phase, the flow is dominated by natural convection; (2) the formation of macrosegregation is caused mainly by the interdendritic fluid flow in the mushy zone; and (3) the shrinkage-induced fluid flow is the major cause for the formation of macrosegregation.

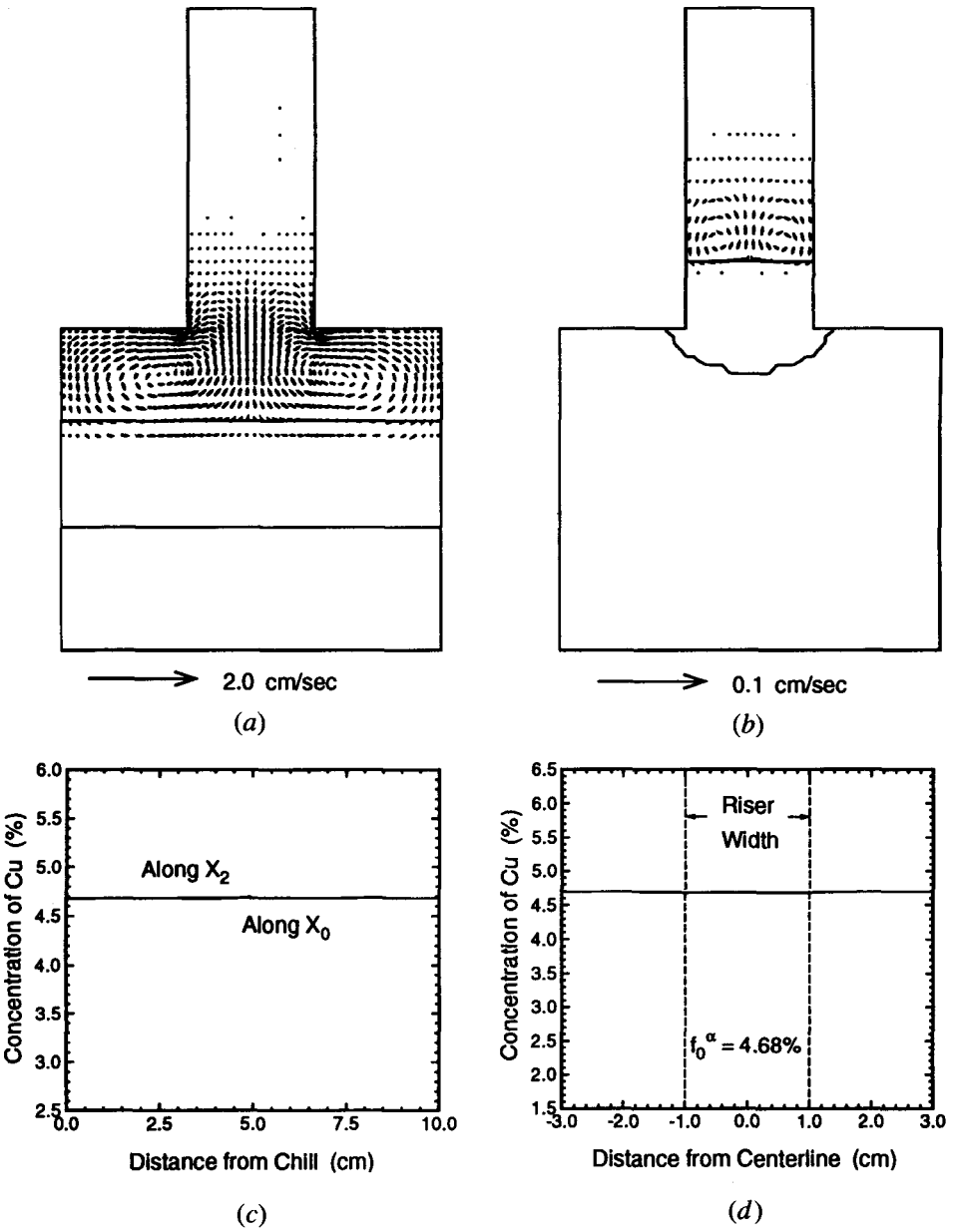

Fig. 9—Velocity vectors: (*a*) at $t = 25$ s and (*b*) at $t = 55$ s; and final solute concentration distributions: (*c*) along X_0 and X_2 axes and (*d*) along the top surface of the casting; if solidification shrinkage is neglected.

D. *Formation of Surface and Interior Macrosegregations*

From this discussion and the results obtained for unidirectional solidification without cross-sectional change,[17] the formation of macrosegregation in a casting cooled from the bottom generally can be divided into two categories: one is the surface segregation (*i.e.*, segregation occurs near the surface of the casting), and the other is the interior segregation (*i.e.*, segregation occurs in the interior of the casting). For each category, both positive and negative segregations can be formed. For example, the inverse segregation (a positive segregation) and the segregation (positive or negative) along the top shoulder of the casting discussed previously in Section III–A (Figure 6) belong to the surface segregation. There are two conditions under which the surface segregation can occur: (1) the casting near the wall is in the mushy state; and (2) there is a fluid flow against or away from an "impermeable wall". The positive surface segregation is caused when interdendritic fluid with higher solute concentration flows toward the wall. The solute is discarded and accumulated near the "dead end" where the flow ceases. Hence, the positive surface segregation can also be called "dead-end segregation." Inverse segregation and positive segregation at the top corners of the casting are dead-end segregation. On the other hand, a negative surface segregation is created if the solute is swept away from the surface. The negative segregation along the curve from point b to point c in Figure 6 belongs to the negative surface segregation. The fluid flow resulting in the formation of surface segregation can be caused by solidification shrinkage, as in

the case of inverse segregation, or by the change of cross section, as in the segregation along the top shoulder of the casting.

Interior segregation within a casting is formed when there is a sudden change of solidification rate, resulting in an increase or decrease of the size of the mushy zone. For UDS without cross-sectional change, Flemings *et al.*[7] and Diao and Tsai[17] have found that an abrupt change of the width of the mushy zone (which is equivalent to a sudden change of the local solidification rate) due to a sudden change of cooling condition at the bottom of the casting could result in the formation of positive or negative segregation. A sudden increase of the size of the mushy zone (*i.e.*, decrease in the solidification rate) will result in a positive segregation, while a negative segregation can be caused by a sudden increase in solidification rate. This principle also is applicable to the present study having a sudden change of cross section. To confirm this, the positions of the liquidus front, solidus front, and the size of the mushy zone along the centerline of the casting are plotted in Figure 10. It is seen that the change of cross section decreases the width of the mushy zone and therefore increases the local solidification rate around the under-riser region, resulting in the formation of negative segregation. In fact, a sudden increase of solidification rate in the region near the casting-riser junction is easily understandable, as less heat content is supplied by the smaller riser than by the casting. It is interesting to note that a change of solidification rate in the casting can be achieved by the change of thermal conditions at the boundary and/or by the change of casting geometry.

E. *Effect of Riser Size on the Formation of Macrosegregation*

Figure 11 shows the final solute distributions along the X_0 and X_2 axes in the vertical direction and along the top surface of the casting in the horizontal direction when the riser size is halved and the other conditions remain the same as shown in Figure 1. It is seen that the negative segregation is more severe than that in Figure 7. The results are consistent with our previous arguments that, to feed solidification shrinkage, a smaller riser will result in greater interdendritic flow velocities near the casting-riser intersections, leading to more solute being swept away. Similar results should be obtained if the casting width is increased for the same size of the riser.

F. *Effect of Cooling Rate on the Formation of Macrosegregation*

The heat extraction rate at the bottom of the casting can be increased or decreased by changing the effective convection heat transfer coefficient between the casting and the chill. Figure 12 shows the final solute distributions for the solidified casting when the heat transfer coefficient is decreased from 0.08 to 0.02 W/(cm^2 K). It is seen that both the inverse segregation and under-riser segregation are more severe, and the band width along X_0 appears greater than that shown in Figure 7. The explanation of this phenomenon is straightforward, as a smaller cooling rate causes a wider mushy zone,

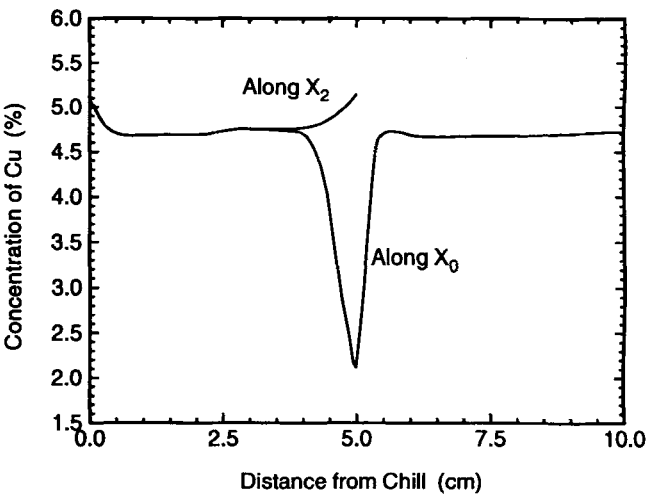

Fig. 11—Predicted solute concentration distribution along X_0 and X_2 axes in the casting with a smaller riser size.

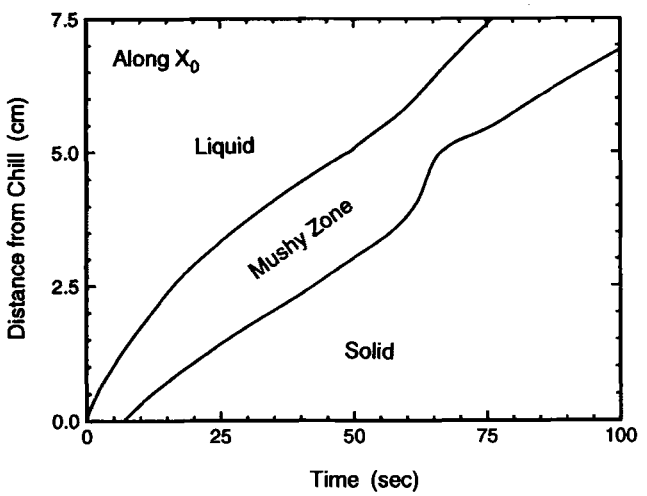

Fig. 10—Positions of the liquidus and solidus fronts as functions of time along axis X_0.

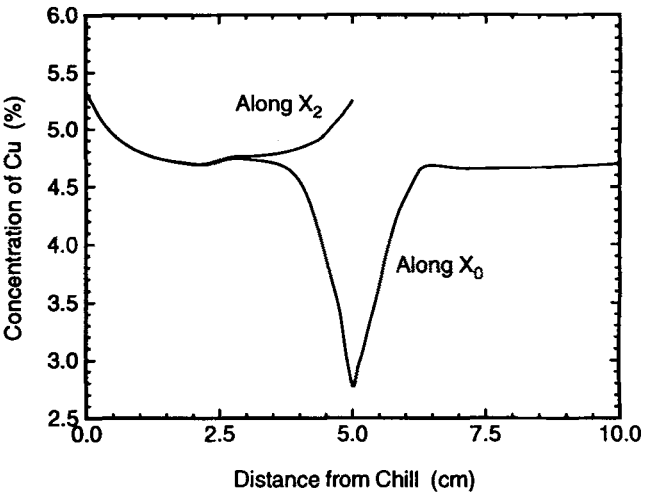

Fig. 12—Predicted solute concentration distribution along X_0 and X_2 axes in the casting with a lower heat extraction rate.

and more time is available for the interdendritic fluid flow to carry more solute away from the casting-riser intersections. The formation of more severe inverse segregation in UDS due to a lower heat extraction rate at the bottom of the casting was discussed in the previous article.[16]

IV. CONCLUSIONS

Fluid flow and its effects on the formation of macrosegregation in an Al-Cu ingot with a cross-sectional change from the riser to the casting have been investigated numerically. The fluid flow is caused by natural convection and solidification shrinkage and is further complicated by the change of cross section. The major conclusions from the present study can be summarized as follows:

1. Fluid flow in the liquid region is influenced by natural convection due to temperature gradients, but the flow in the mushy zone is determined mainly by solidification shrinkage, which is the major cause for the formation of macrosegregation.
2. Inverse segregation at the bottom of the casting, negative segregation around the under-riser region, and positive segregation near the top corners of the casting are found. However, the negative under-riser segregation is much more severe than the other segregations.
3. The different segregations can be well explained by the flow of solute-rich interdendritic fluid and a sudden change of local solidification rate in the mushy zone. The inverse segregation and the segregation along the top shoulder of the casting can be classified as surface segregation caused by the flow of solute-rich liquid against or away from the wall surface. In the present study, the flow is induced by the combined effects of solidification shrinkage and change of cross section. On the other hand, the under-riser segregation is a kind of interior segregation caused by a sudden change of the local solidification rate in the mushy zone due to the change of the cross section.
4. A smaller riser size and a lower heat extraction rate at the bottom of the casting increase the severity of macrosegregation in the casting.
5. The predicted results compare favorably with the available experimental data and previous theoretical predictions.

NOMENCLATURE

c	specific heat
C	coefficient in Eqs. [2] through [3], defined in Eq. [9]
c_1	permeability coefficient, defined in Eq. [8]
d	dendrite arm spacing
D	mass-diffusion coefficient
f	mass fraction
g	volume fraction or gravitational acceleration
h	enthalpy
h_c	effective convection heat transfer coefficient between casting and chill
H	latent heat
k	thermal conductivity
k_p	equilibrium partition ratio
K	permeability function, defined in Eq. [8]
p	pressure
t	time
T	temperature
T_m	fusion temperature at zero solute concentration
u	velocity component in the x-direction
v	velocity component in the y-direction
$\mathbf{V}$	velocity vector
x, y	Cartesian coordinates

Greek Symbols

β_S	solutal expansion coefficient
β_T	thermal expansion coefficient
μ	dynamic viscosity
ρ	density

Subscripts

0	initial value
c	chill
e	eutectic
l	liquid phase
m	fusion
r	relative to solid phase
s	solid phase

Superscript

α	constituent of alloy

ACKNOWLEDGMENT

The authors are grateful for the partial support by the Air Force Office of Scientific Research under Contract No. F49620-88-C-0053/SB5881-0378.

REFERENCES

1. R.J. McDonald and J.D. Hunt: *Trans. TMS-AIME*, 1969, vol. 245, pp. 1993-97.
2. N. Streat and F. Weinberg: *Metall. Trans.*, 1974, vol. 5, pp. 2539-48.
3. M.C. Flemings: *Solidification Processing*, McGraw-Hill, Inc., New York, NY, 1974, pp. 214-58.
4. E. Scheil: *Metallforschung*, 1947, vol. 2, pp. 69-75.
5. J.S. Kirkaldy and W.V. Youdelis: *Trans. TMS-AIME*, 1958, vol. 212, pp. 833-40.
6. M.C. Flemings and G.E. Nereo: *Trans. TMS-AIME*, 1967, vol. 239, pp. 1449-61.
7. M.C. Flemings, R. Mehrabian, and G.E. Nereo: *Trans. TMS-AIME*, 1968, vol. 242, pp. 41-49.
8. M.C. Flemings and G.E. Nereo: *Trans. TMS-AIME*, 1968, vol. 242, pp. 50-55.
9. R. Mehrabian, M. Keane, and M.C. Flemings: *Metall. Trans.*, 1970, vol. 1, pp. 1209-20.
10. T. Fujii, D.R. Poirier, and M.C. Flemings: *Metall. Trans. B*, 1979, vol. 10B, pp. 331-39.
11. C. Beckermann and R. Viskanta: *PCH, PhysicoChem. Hydrodyn.*, 1988, vol. 10, pp. 195-213.
12. W.D. Bennon and F.P. Incropera: *Int. J. Heat Mass Transfer*, 1987, vol. 30, pp. 2161-70.
13. D.G. Neilson and F.P. Incropera: *Int. J. Heat Mass Transfer*, 1991, vol. 34, pp. 1717-32.

14. K.C. Chiang and H.L. Tsai: *Int. J. Heat Mass Transfer*, 1992, vol. 35, pp. 1763-70.
15. K.C. Chiang and H.L. Tsai: *Int. J. Heat Mass Transfer*, 1992, vol. 35, pp. 1771-78.
16. Q.Z. Diao and H.L. Tsai: *Metall. Trans. A*, 1993, vol. 24A, pp. 963-73.
17. Q.Z. Diao and H.L. Tsai: *Int. J. Heat Mass Transfer*, 1993, vol. 36, pp. 4299-4305.
18. P.C. Carman: *Trans. Inst. Chem. Eng.*, 1937, vol. 15, pp. 150-66.
19. K. Kubo and R.D. Pehlke: *Metall. Trans. B*, 1985, vol. 16B, pp. 359-66.
20. G.S. Beavers and E.M. Sparrow: *J. Appl. Mech.*, 1969, vol. 36, pp. 711-14.
21. T. Takahashi, M. Kudoh, and K. Yodoshi: *Trans. Jpn. Inst. Met.*, 1979, vol. 43, pp. 1086-91.
22. J.H. Chen and H.L. Tsai: *Int. J. Heat Mass Transfer*, 1993, vol. 36, pp. 3069-75.
23. I. Ohnaka and M. Matsumoto: *Trans. Iron Steel Inst. Jpn.*, 1987, vol. 14, pp. 86-93.